nature nanotechnology

LETTERS

PUBLISHED ONLINE: 31 MARCH 2013 | DOI: 10.1038/NNANO.2013.41

Nanowire liquid pumps

Jian Yu Huang[1†], Yu-Chieh Lo[2,3†], Jun Jie Niu[2], Akihiro Kushima[2], Xiaofeng Qian[2], Li Zhong[4], Scott X. Mao[4,5] and Ju Li[2*]

The ability to form tiny droplets of liquids[1–6] and control their movements[7–10] is important in printing or patterning[1,2], chemical reactions[10–12] and biological assays[9,10,13,14]. So far, such nanofluidic[15,16] capabilities have principally used components such as channels[9,10], nozzles[1,6] or tubes[17–22], where a solid encloses the transported liquid. Here, we show that liquids can flow along the outer surface of solid nanowires at a scale of attolitres per second and the process can be directly imaged with *in situ* transmission electron microscopy. Microscopy videos show that an ionic liquid can be pumped along tin dioxide, silicon or zinc oxide nanowires as a thin precursor film or as beads riding on the precursor film. Theoretical analysis suggests there is a critical film thickness of ~10 nm below which the liquid flows as a flat film and above which it flows as discrete beads. This critical thickness is the result of intermolecular forces between solid and liquid, which compete with liquid surface energy and Rayleigh–Plateau instability.

According to the theory of solid–liquid interactions[23,24], in the complete wetting scenario (contact angle 0°) a liquid film of thickness ~1–10 nm, called a precursor film, can creep on solid surfaces with certain spatial-temporal features[25]. This thickness is a direct signature of intermolecular forces between solid and liquid, and the spreading dynamics may be further controlled by (i) applying an electrical bias (electrokinetic flow[1,5,9,10,15,16,26]), (ii) tuning the taper angle of individual nanowires, which creates a gradient in the contact area, or (iii) changing the topological connectivity of multiple nanowires, which controls the 'landscape' of dry surface areas and thus the total capillary energy[27]. The gravitational effect can be ignored in such a nanowire–fluidic system.

The ionic liquid 1,2-dimethyl-3-propylimidazolium (DMPI)-bis(trifluoromethylsulphonyl)imide (TFSI) has low vapour pressure and survives the high vacuum inside a transmission electron microscope (TEM)[28], thus allowing *in situ* studies of liquid–solid wetting behaviour at high spatial resolution. Our experiments were conducted inside a Tecnai F30 TEM with a line resolution of 0.14 nm, and equipped with a Nanofactory scanning tunnelling microscope (STM)-TEM holder. SnO_2, ZnO or silicon nanowires were glued to a gold rod using conductive epoxy (Chemtronics, CW2400), and the rod was attached to a three-dimensional piezo manipulator (Fig. 1a). A drop of ionic liquid was placed on the tip of a gold STM probe, and the entire set-up was loaded into the TEM. The nanowires were then manipulated to approach the ionic liquid. Figure 1b–e shows the formation of discrete liquid beads on two SnO_2 nanowires. As seen in Supplementary Movies S1 and S2, the ionic liquid accumulates at a new depository that is micrometres away from the main liquid reservoir. The electron beam intensity was limited to $<1\times10^{-3}$ A cm^{-2} in the TEM chamber (0.62 e Å^{-2} s^{-1}), so the influence of the electron beam on the nanofluid was small[29]. Details of the experimental set-up and analyses of the electron beam effect are presented in the Supplementary Information. Higher-resolution TEM images of the nanowire surface between beads show a smooth layer of liquid film (Fig. 1f) with a thickness of ~10 nm. This is the molecular-scale precursor film[23,24] that has long been predicted in theory, now caught in hydrodynamic flow on video.

According to classic Rayleigh–Plateau analysis[30], a liquid cylinder of radius profile $r(z)=b$ will develop an instability at wavelength $\Delta z\approx 9b$. The same argument also applies to a liquid film of thickness $e(z)$ coating a solid nanowire of uniform radius b, because a small variation in the radius profile $\delta e(z)$ should give an identical change in liquid surface energy as in a fully liquid jet. However, such instability is suppressed in Fig. 1f, where the liquid film thickness $e(z)$ remains highly uniform and flat. This is because when $e(z)$ decreases to a thickness of ~10 nm, the liquid will not only feel the Young–Laplace pressure

$$\gamma\left[\frac{1}{(b+e)[1+(\partial_z e)^2]^{1/2}}-\frac{\partial_z^2 e}{[1+(\partial_z e)^2]^{3/2}}\right]$$

due to the liquid surface energy γ that destabilizes the film uniformity, but will also start to feel a direct intermolecular attraction with the solid, which stabilizes the uniform film. In other words, Fig. 1f is direct evidence of rather long-range quantum dispersion forces between liquid molecules and the solid nanowire at a separation of ~10 nm. For simplicity, we assume the liquid–solid interaction energy per area takes the form $W(e)=\text{const}+A/12\pi e^2$ due to non-retarded van der Waals attraction[31], where A is the Hamaker constant typically on the order of 1×10^{-19} J. $W(e)$ acts to thicken the precursor film, and exerts a disjoining pressure $\Pi(e)\equiv -\mathrm{d}W(e)/\mathrm{d}e=A/6\pi e^3$ on the outer liquid surface. These two effects, combined, give an excess molecular chemical potential of

$$\mu=\gamma\Omega\left[\frac{1}{(b+e)[1+(\partial_z e)^2]^{1/2}}-\frac{\partial_z^2 e}{[1+(\partial_z e)^2]^{3/2}}\right]-\frac{\Omega b\Pi(e)}{b+e} \quad (1)$$

versus the bulk liquid, where Ω is the molecular volume (~500 Å^3 for a DMPI–TFSI molecular ion pair). Figure 2a presents a plot, for a uniform film ($\partial_z e=\partial_z^2 e=0$), of the sum of the first (always positive, red dashed line) and third (always negative) terms in equation (1). These two terms compete with each other in the morphological stability analysis, and give rise to two regimes of hydrodynamic flow behaviour: the smooth precursor film flow shown in Fig. 1f, where e is small and uniform, and Rayleigh bead flow where e is large and varying. The transition occurs around a critical

[1]Centre for Integrated Nanotechnologies, Sandia National Laboratories, Albuquerque, New Mexico 87185, USA, [2]Department of Nuclear Science and Engineering and Department of Materials Science and Engineering, Massachusetts Institute of Technology, Cambridge, Massachusetts 02139, USA, [3]Department of Materials Science and Engineering, University of Pennsylvania, Philadelphia, Pennsylvania 19104, USA, [4]Department of Mechanical Engineering and Materials Science, University of Pittsburgh, Pittsburgh, Pennsylvania 15261, USA, [5]Centre for Electron Microscopy, Department of Materials Science and Engineering, Zhejiang University, Hangzhou 310027, China; †These authors contributed equally to this work. *e-mail: liju@mit.edu

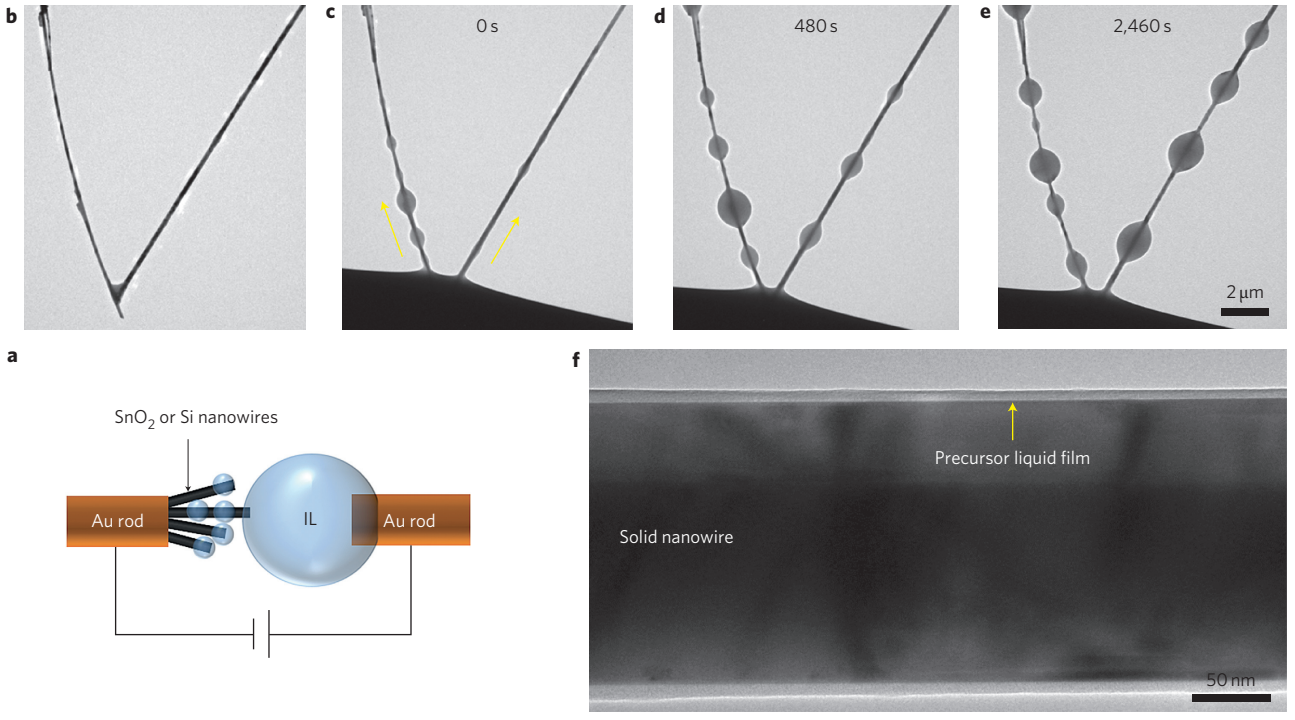

Figure 1 | Ionic liquid beads and flat precursor film. a, Experimental set-up. SnO_2 nanowire powders or silicon nanowires grown on a silicon wafer are glued to a gold rod (diameter, ~280 μm) using conducting silver epoxy (left). The whole nanowire assembly is used as one electrode. The other electrode is a gold STM probe (right). A drop of ionic liquid (IL, middle) is placed on the STM tip. One of the electrodes is attached to a three-dimensional piezo manipulator to enable it to approach the opposite electrode. **b**–**e**, Time-lapse TEM images showing ionic liquid flowing along two SnO_2 nanowires. The diameters of the nanowires on the left and right are 120 nm and 190 nm, respectively. The arrows in **c** shows the bead flow direction. The SnO_2 nanowires were biased at −4 V versus the reference electrode. The growth of beads is seen clearly. **f**, A liquid precursor film with a thickness of ~10 nm wets and flows on a SnO_2 nanowire.

liquid film thickness $e_{\text{PF-RB}} \approx 10$ nm by plugging in parameters estimated for DMPI-TFSI[32] (Fig. 2a). These two flow states (film–bead) co-exist and frequently toggle between one another, as shown in Supplementary Movies S1–S4.

Under the so-called lubrication approximation[23,24], we solved the profile evolution equation $3\eta\Omega(1+e/b)\partial_t e = \partial_z(e^3\partial_z\mu)$ numerically; this is a stiff nonlinear equation where η is the liquid viscosity. The result, starting from a random profile, is shown in Fig. 2b, where a string of co-existing· · ·–film–bead–film–bead–· · ·flow states are obtained. This can be understood by the following. The Rayleigh–Plateau instability develops whenever e becomes large, but instead of breaking up into completely disconnected droplets as for a liquid cylinder, the instability will always get arrested when e becomes thin enough to be stabilized by the van der Waals attraction forces to the solid. From the nanofluidic transport point of view, this arrested development of the Rayleigh–Plateau instability makes for a completely different scenario, because all the beads remain connected by the precursor film, and liquid molecules can flow freely in this thin film layer (Supplementary Movies S1 and S2). An equal-aspect-ratio view of one such liquid bead from our numerical simulation is shown in Fig. 2c. Note that in the full numerical solution the second term in equation (1) depends on $\partial_z^2 e$ and can be negative or positive, thus continuously mediating the transition between precursor film and Rayleigh bead states. As shown in Fig. 1c–e and Supplementary Movies S2–S4, the beads on the SnO_2 nanowires exhibit essentially self-similar shapes, but the beads vary greatly in size. Molecular dynamics simulations of a non-volatile polymeric liquid on a solid nanowire (Fig. 2d–f and Supplementary Movies S10 and S11) confirm the same physics as the continuum description (Fig. 2a–c) discussed above.

Moreover, droplet flow behaviour is sensitive to the applied voltage. When the bias voltage on the nanowire is reversed, the motion of the beads can also be reversed (Supplementary Movie S2). Without applying negative bias, the precursor film spreads on the nanowire surface (Fig. 1f), but beads may not form or flow. A wire taper shape effect is also observed. A silicon nanowire of length ~11 μm was tapered so as to have base and tip diameters of 300 nm and 150 nm, respectively. The first bead moved with a speed of 0.75 μm s^{-1} up the nanowire. When the wider end of the nanowire was in contact with the ionic liquid, the ionic liquid flowed much more slowly (Supplementary Fig. S1h–l) than when the thinner end was in contact with the ionic liquid (Supplementary Fig. S1a–g). If the bias voltage of the nanowire is changed from negative to positive, the liquid can change its flow rate or cease flowing altogether. In Supplementary Fig. S1, the average flow rate is 50 al s^{-1}. This can be compared with the flow rates in Supplementary Movies S1 (Fig. 1f) and S2, which are 20 al s^{-1} and 84 al s^{-1}, respectively, both with no beads. Thus the formation of beads does not have a tremendous impact on the net flow rate of liquid along nanowires.

Hypodermic syringe needles and glass micropipettes are well-known tubular instruments in medicine and biology for extracting, holding and transferring liquids, with inner diameters of ~100 μm and 1 μm, respectively. Here, we would like to demonstrate that at a 0.1 μm scale diameter, solid nanowires can still extract and hold liquids as effectively as hollow tubules. We first show that liquids can be pumped rapidly along a uniform ZnO nanowire from the liquid reservoir to a graphene substrate (Fig. 3a,b, Supplementary Movie S5). The flow rate approaches ~10–100 al s^{-1} depending on the applied voltage. This liquid delivery phenomenon is not limited to ionic liquid, as we have also observed similar phenomena using deionized water under an optical microscopy (Supplementary Fig. S2, Supplementary Movie S6). Thus, the film–bead co-existence is an intrinsic behaviour of fluid transport on the nanowire surface. Based on this result, a simple nanofluid–nanowire transportation

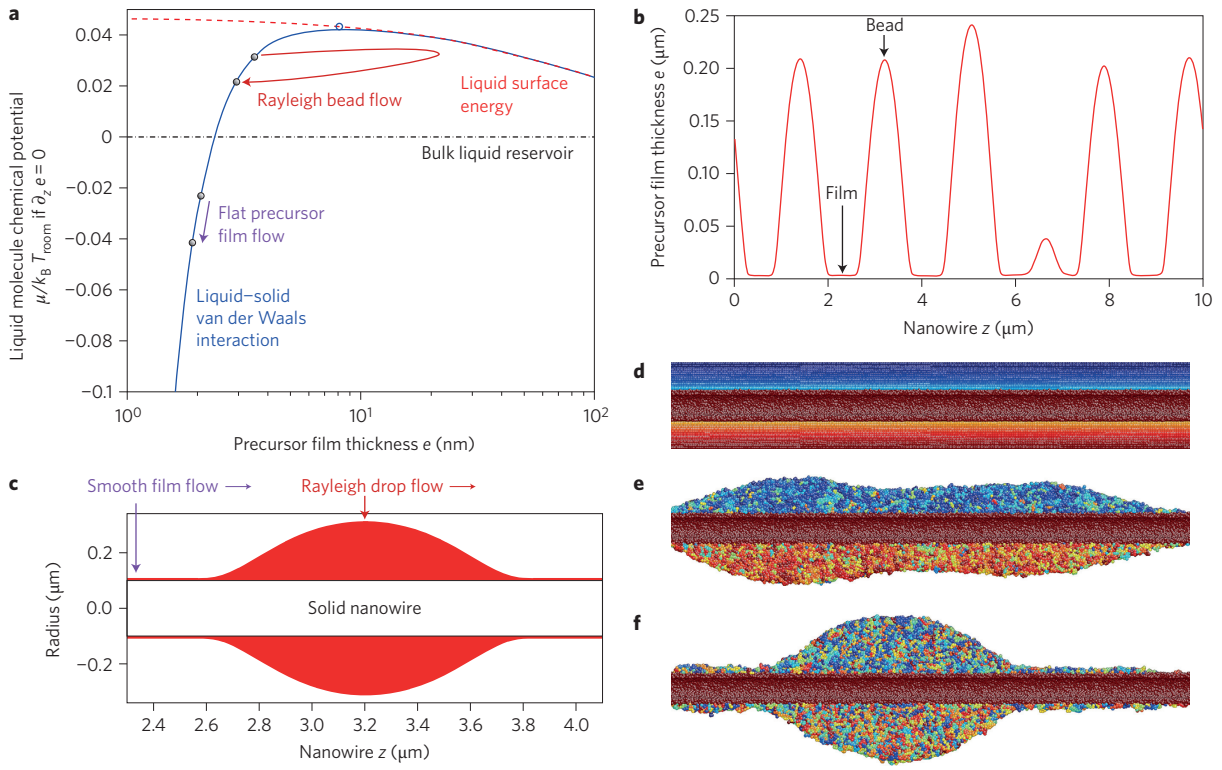

Figure 2 | Modelling and simulations. a, A semilogarithmic plot of the chemical potential of a liquid molecule as a function of precursor film thickness e, on a nanowire with a radius of $b = 100$ nm. **b**, Numerical solution of $3\eta\Omega(1 + e/b)\partial_t e = \partial_z(e^3\partial_z\mu)$ on the nanowire of radius $b = 100$ nm and length $z = 10$ μm. Note that the beads are connected by a thin flat precursor film a few nanometres thick. This plot does not have equal aspect ratio. **c**, Amplified view of the liquid profile for the solution in **b** around $z = 3$ μm, with equal aspect ratio. **d**–**f**, Molecular dynamics simulation of a polymeric liquid (each chain has $N = 10$ monomers) coating a solid nanowire (red) with $b = 2.5$ nm, forming both precursor films and beads. Each chain maintains the same colour as in **d**, thereby illustrating molecular diffusion.

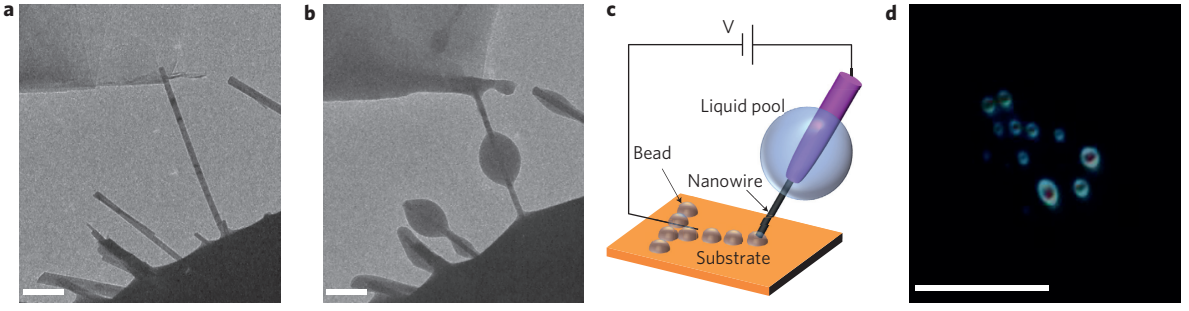

Figure 3 | Transport and patterning of liquids by nanowire. a,**b**, TEM images of ionic liquid delivery from a reservoir to a piece of graphene using a ZnO nanowire (Supplementary Movie S5). Scale bars, 0.5 μm. **c**, Schematic illustration of a nanofluid–nanowire transportation device for patterning. **d**, An optical micrograph of a deionized water pattern produced by a nanofluid-SnO_2 nanowire device. Scale bar, 4 μm.

device was designed, as shown schematically in Fig. 3c, which allows us to pattern liquid droplets on a substrate (Fig. 3d).

Liquid can be temporarily stored at intersections with other nanowires (Fig. 4a–k and Supplementary Movie S7). Such a depository exists because a nanowire intersection has excess solid surface area and provides a trap state for the liquid. The capacity of such depositories is on the order of 10–1,000 al. We also constructed a complex liquid flow pattern guided by an 'inverted forest' of silicon nanowires (Fig. 4l–q, Supplementary Movies S8 and S9). Liquid was pumped up as in a root system, and the driving force was provided by the huge 'dry' areas of the forest on top and the relatively small intake at the bottom, creating a 'traffic jam' of liquid droplets. Some depositories periodically oscillated in the amount of liquid stored (Supplementary Movie S9), like a pumping heart, indicating hysteresis in the networked fluid flow.

A recent high-resolution TEM study indicated crystalline short-range order in four ionic liquids at room temperature with a $\lambda \approx 1$–10 nm spatial extent and long lifetimes[33]. Many aspects of liquid behaviour are expected to be influenced by this. In particular, when the liquid film thickness e approaches the crystalline short-range order cluster size, continuum fluid dynamics models such as the lubrication equation are expected to break down, as continuum-level quantities like the viscosity become ill-defined. Such a continuum model was nonetheless used in this work for simplicity, and is expected to work well quantitatively in the beaded region where $e(z) \gg \lambda$, but less well in the thin precursor film region.

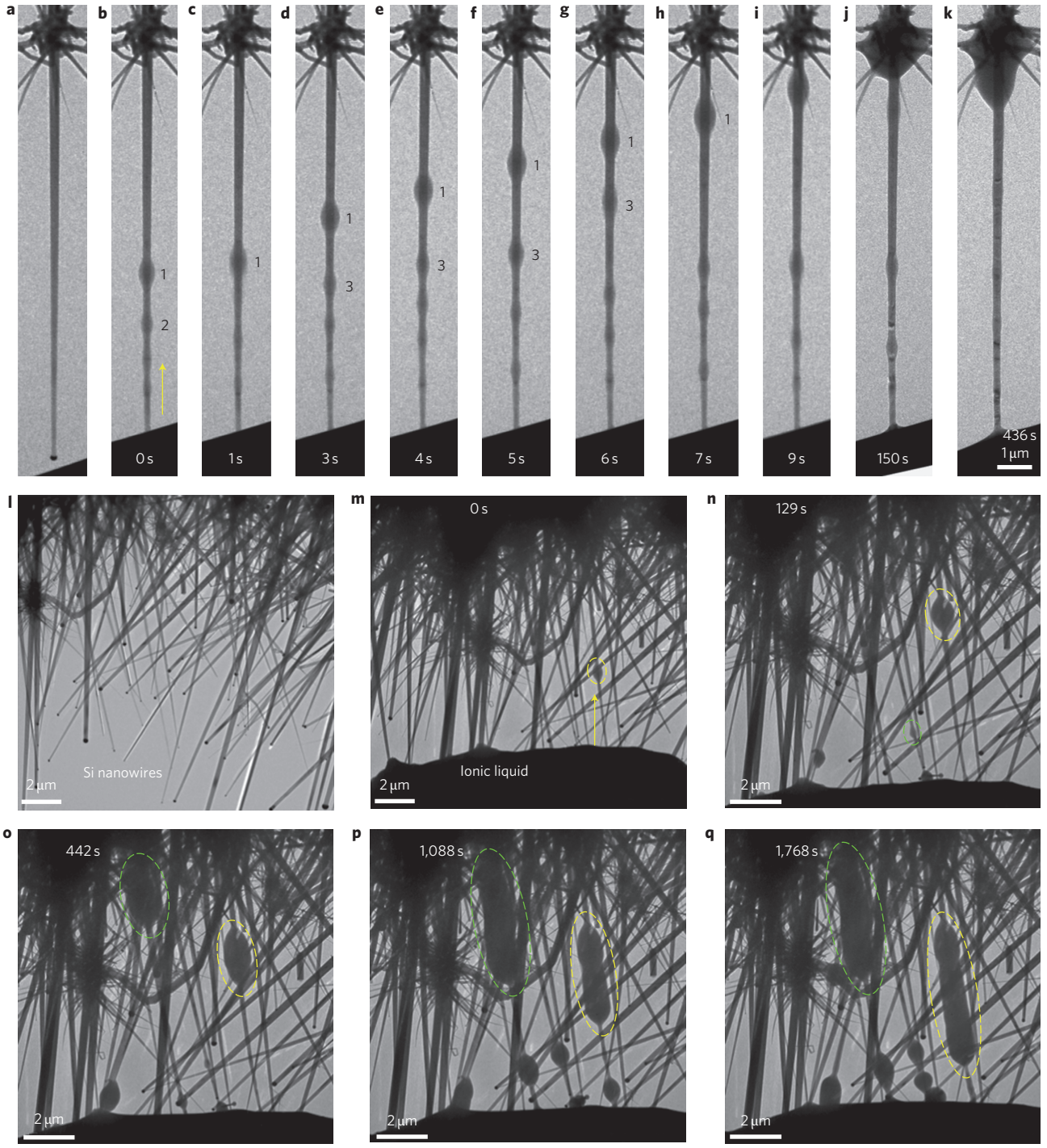

Figure 4 | Nanowire network nanofluidics. a–k, Ionic liquid beads flow along a silicon nanowire. The ionic liquid beads stop at a nanowire intersection on top of the nanowire and accumulate there as a temporary depot (Supplementary Movie S7). The black numbers in **b–h** indicate individual beads on the nanowire. **l–q**, Ionic liquid beads flow along multiple silicon nanowires (Supplementary Movies S8 and S9). Green and yellow ellipses outline two sausage-on-a-stick-shaped ionic liquid deposits on the silicon nanowires.

Note, however, that features like film–bead co-existence are based on the energetic part of the model, equation (1), which should be more robust than the fluid dynamics model.

Received 2 August 2012; accepted 21 February 2013; published online 31 March 2013

References

1. Park, J. U. *et al.* High-resolution electrohydrodynamic jet printing. *Nature Mater.* **6,** 782–789 (2007).
2. Ferraro, P., Coppola, S., Grilli, S., Paturzo, M. & Vespini, V. Dispensing nano–pico droplets and liquid patterning by pyroelectrodynamic shooting. *Nature Nanotech.* **5,** 429–435 (2010).
3. Gañán-Calvo, A. M., González-Prieto, R., Riesco-Chueca, P., Herrada, M. A. & Flores-Mosquera, M. Focusing capillary jets close to the continuum limit. *Nature Phys.* **3,** 737–742 (2007).
4. Loscertales, I. G. *et al.* Micro/nano encapsulation via electrified coaxial liquid jets. *Science* **295,** 1695–1698 (2002).
5. Collins, R. T., Jones, J. J., Harris, M. T. & Basaran, O. A. Electrohydrodynamic tip streaming and emission of charged drops from liquid cones. *Nature Phys.* **4,** 149–154 (2008).

6. Utada, A. S. *et al.* Monodisperse double emulsions generated from a microcapillary device. *Science* **308,** 537–541 (2005).
7. Velev, O. D., Prevo, B. G. & Bhatt, K. H. On-chip manipulation of free droplets. *Nature* **426,** 515–516 (2003).
8. Zheng, Y. M. *et al.* Directional water collection on wetted spider silk. *Nature* **463,** 640–643 (2010).
9. Teh, S. Y., Lin, R., Hung, L. H. & Lee, A. P. Droplet microfluidics. *Lab on a Chip* **8,** 198–220 (2008).
10. Song, H., Chen, D. L. & Ismagilov, R. F. Reactions in droplets in microflulidic channels. *Angew. Chem. Int. Ed.* **45,** 7336–7356 (2006).
11. Millman, J. R., Bhatt, K. H., Prevo, B. G. & Velev, O. D. Anisotropic particle synthesis in dielectrophoretically controlled microdroplet reactors. *Nature Mater.* **4,** 98–102 (2005).
12. Anzenbacher, P. & Palacios, M. A. Polymer nanofibre junctions of attolitre volume serve as zeptomole-scale chemical reactors. *Nature Chem.* **1,** 80–86 (2009).
13. Fenn, J. B. Electrospray wings for molecular elephants. *Angew. Chem. Int. Ed.* **42,** 3871–3894 (2003).
14. Tavana, H. *et al.* Nanolitre liquid patterning in aqueous environments for spatially defined reagent delivery to mammalian cells. *Nature Mater.* **8,** 736–741 (2009).
15. Sparreboom, W., van den Berg, A. & Eijkel, J. C. T. Principles and applications of nanofluidic transport. *Nature Nanotech.* **4,** 713–720 (2009).
16. Schoch, R. B., Han, J. Y. & Renaud, P. Transport phenomena in nanofluidics. *Rev. Mod. Phys.* **80,** 839–883 (2008).
17. Whitby, M. & Quirke, N. Fluid flow in carbon nanotubes and nanopipes. *Nature Nanotech.* **2,** 87–94 (2007).
18. Rossi, M. P. *et al.* Environmental scanning electron microscopy study of water in carbon nanopipes. *Nano Lett.* **4,** 989–993 (2004).
19. Naguib, N. *et al.* Observation of water confined in nanometer channels of closed carbon nanotubes. *Nano Lett.* **4,** 2237–2243 (2004).
20. Mattia, D. & Gogotsi, Y. Static and dynamic behavior of liquids inside carbon nanotubes. *Microfluid Nanofluid* **5,** 289–305 (2008).
21. Kim, B. M., Sinha, S. & Bau, H. H. Optical microscope study of liquid transport in carbon nanotubes. *Nano Lett.* **4,** 2203–2208 (2004).
22. Chen, J. Y., Kutana, A., Collier, C. P. & Giapis, K. P. Electrowetting in carbon nanotubes. *Science* **310,** 1480–1483 (2005).
23. De Gennes, P. G. Wetting—statics and dynamcis. *Rev. Mod. Phys.* **57,** 827–863 (1985).
24. Bonn, D., Eggers, J., Indekeu, J., Meunier, J. & Rolley, E. Wetting and spreading. *Rev. Mod. Phys.* **81,** 739–805 (2009).
25. Brochard-Wyart, F., di Meglio, J-M. & Quéré, D. Theory of the dynamics of spreading of liquids on fibers. *J. Phys. France* **51,** 293–306 (1990).
26. Lee, S., An, R. & Hunt, A. J. Liquid glass electrodes for nanofluidics. *Nature Nanotech.* **5,** 412–416 (2010).
27. Moosavi, A., Rauscher, M. & Dietrich, S. Motion of nanodroplets near edges and wedges. *Phys. Rev. Lett.* **97,** 236101 (2006).
28. Huang, J. Y. *et al. In situ* observation of the electrochemical lithiation of a single SnO_2 nanowire electrode. *Science* **330,** 1515–1520 (2010).
29. Mirsaidov, U. M., Zheng, H., Bhattacharya, D., Casana, Y. & Matsudaira, P. Direct observation of stick–slip movements of water nanodroplets induced by an electron beam. *Proc. Natl Acad. Sci. USA* **109,** 7187–7190 (2012).
30. Rayleigh, L. On the capillary phenomena of jets. *Proc. R. Soc. Lond.* **29,** 71–97 (1879).
31. Israelachvili, J. N. *Intermolecular and Surface Forces with Applications to Colloidal and Biological Systems* 2nd edn (Academic, 1992).
32. Zhang, S. J., Sun, N., He, X. Z., Lu, X. M. & Zhang, X. P. Physical properties of ionic liquids: database and evaluation. *J. Phys. Chem. Ref. Data* **35,** 1475–1517 (2006).
33. Chen, S., Kobayashi, K., Kitaura, R., Miyata, Y. & Shinohara, H. Direct HRTEM observation of ultrathin freestanding ionic liquid film on carbon nanotube grid. *ACS Nano* **5,** 4902–4908 (2011).

Acknowledgements

This work was supported by a Laboratory Directed Research and Development (LDRD) project at Sandia National Laboratories (SNL) and by the Science of Precision Multifunctional Nanostructures for Electrical Energy Storage (NEES), an Energy Frontier Research Centre funded by the US Department of Energy (DOE), Office of Science, Office of Basic Energy Sciences (BES) under award DESC0001160. This work was performed, in part, at the Sandia-Los Alamos Centre for Integrated Nanotechnologies (CINT), a US Department of Energy, Office of Basic Energy Sciences user facility. Sandia National Laboratories is a multiprogramme laboratory operated by Sandia Corporation, a wholly owned subsidiary of Lockheed Martin, for the US Department of Energy's National Nuclear Security Administration (under contract no. DE-AC04-94AL85000). Y.C.L., J.J.N., A.K., X.F.Q. and J.L. acknowledge support by the National Science Foundation (NSF; grant DMR-1120901). J.Y.H. thanks Chongmin Wang and Wu Xu for providing the ionic liquid and the SnO_2 nanowires. L.Z. and S.X.M. acknowledge support from the NSF (grant CMMI 08 010934) through University of Pittsburgh.

Author contributions

J.Y.H. and J.L. conceived and designed the experiments. J.Y.H., A.K. and L.Z. performed the *in situ* TEM experiments. Y.C.L. and J.L. carried out modelling and simulations. L.Z. and S.X.M. performed TEM imaging analysis. J.J.N. and Y.C.L. performed the optical microscopy experiment. J.J.N., A.K. and X.F.Q. also contributed to the Supplementary Information. Y.C.L., J.Y.H. and J.L. wrote the paper. All authors analysed the data, discussed the results and commented on the manuscript.

Additional information

Supplementary information is available in the online version of the paper. Reprints and permissions information is available online at www.nature.com/reprints. Correspondence and requests for materials should be addressed to J.L.

Competing financial interests

The authors declare no competing financial interests.